

A 3D electron fluid model to study magnetic field effects on an expanding plasma thruster plume

F. Cichocki¹, M. Merino¹, E. Ahedo¹

¹Equipo de Propulsión Espacial y Plasmas, Universidad Carlos III de Madrid, Leganés, Spain,
Email: filippo.cichocki@uc3m.es.

KEYWORDS:

EP2PLUS, hybrid, PIC, magnetized electrons

ABSTRACT

This paper presents the extension of a hybrid particle-in-cell/fluid code, primarily developed to study plasma plumes expansion and their interaction with the emitting satellite. The original electron fluid model of the code, which already retains the effects of electron collisions with the heavy species (ions and neutrals) is extended to include the effects of an applied magnetic field. The new model is used to analyze the expansion of a plasma plume into vacuum, under the action of the geomagnetic field in low Earth orbit. Different angles between the plume axis and the magnetic field are considered and the results are discussed. An axial magnetic field (parallel to the plume axis) induces a visible plume channeling, while off-axis magnetic fields produce non-trivial and non-symmetric deformation of the plume cross section with a negligible deflection.

1. INTRODUCTION

The complex interaction between an expanding plasma thruster plume and the emitting spacecraft is a topic of great interest in the plasma propulsion community. In fact, it is crucial for satellite integration, in which the negative impact of the emitted plasma plume on sensitive surfaces has to be minimized, but also in other contexts like that of the ion beam shepherd [1–4], a space debris removal technique, where a target object is relocated to a different orbit by means of the ion push of a plasma thruster plume directed towards it. The large amount of new plasma plume codes that have been published in recent years demonstrate such an increasing interest. These codes can be roughly divided into 3 categories: (i) multi-fluid codes [5–10], where both electrons and heavy particles are modeled with a single or multiple fluids, (ii) hybrid codes [11–22], in which electrons are treated as a fluid, while heavy particles are modeled as macro-particles of a particle-in-cell (PIC) sub-model, and (iii) full-PIC codes [23–28], where both electrons and heavy particles (typically only the ions, with the neutrals approximated as a back-

ground fluid) are simulated as macro-particles.

As described in Refs. [29] and [30], hybrid codes represent the best compromise between accuracy and computational cost, when dealing with the study of plasma plume expansions. The EP2PLUS code (Extensible Parallel Plasma PLUme Simulator), is a three-dimensional hybrid-PIC code, which was firstly presented at the 2016 space propulsion conference [31]. This code has undergone important improvements since then [29, 30], especially for what concerns the electron fluid model. While the electron fluid closure is still carried out at the level of the momentum balance equation by either considering a kinetically-based electron pressure tensor (from fully-kinetic studies) or assuming polytropic electrons, collisional effects are fully retained and the resulting model permits computing the electron current density in the plume. Moreover, a non-neutrality criterion is used to dynamically split the simulation domain into quasineutral and non-neutral regions, thus enabling the study of very low density plasmas, like that in the vicinity of the S/C surfaces or in the peripheral region of the main plasma plume.

A magnetic field can affect the expansion of the plasma plume. This phenomenon has received a modest attention in the past, mainly by Korsun et al. [32], who indicated plume channeling if the magnetic field is aligned with the plume axis (the reduced off-axis mobility of the electrons reduces the radial ambipolar electric field and hence the plume divergence increase downstream), and the asymmetric lateral expansion of the plume if it is oblique (i.e. at an angle with the plume axis).

In the present work, the electron fluid model of the EP2PLUS code is extended to include the effects of a mild magnetic field, like the Earth's magnetic field (or any other externally-applied magnetic field, such as that generated by the thruster itself). This extension permits studying the non-trivial effects of a magnetic field on a plasma plume expansion.

The rest of the paper is structured as follows. The extension of the electron fluid model to a magnetized plasma plume expansion is described in Sec. 2. Simulation results for different applied magnetic field orientations and strengths are reported

and discussed in Sec. 3. Finally, conclusions and future work are summarized in Sec. 4.

2. THE MAGNETIZED PLUME MODEL

For a stationary ($\partial/\partial t = 0$) and massless ($m_e \approx 0$) electron fluid, the electron momentum balance equation can be written as:

$$0 = -\nabla \cdot \mathcal{P}_e - en_e (\mathbf{E} + \mathbf{u}_e \times \mathbf{B}) - \sum_{s=1}^L \nu_{es} m_e n_e (\mathbf{u}_e - \mathbf{u}_s) \quad (\text{Eq. 1})$$

where \mathcal{P}_e is the electron pressure tensor, n_e is the electron number density, m_e is the electron mass, \mathbf{u}_e is the electron fluid velocity, \mathbf{E} is the electric field, \mathbf{B} is an externally applied magnetic induction field, L is the number of heavy particle populations (with which the electrons can collide), ν_{es} is the momentum transfer collision frequency of the electrons with the generic s^{th} particle population, which features a fluid velocity \mathbf{u}_s .

Let $\mathbf{j}_e = -en_e \mathbf{u}_e$ and $\mathbf{j}_i = \sum_{s=1}^L e Z_s n_s \mathbf{u}_s$ be the electron and ion current density (Z_s and n_s are respectively the charge number and the number density of the generic s^{th} particle population). We define the driving current density [29] as:

$$\mathbf{j}_d = \mathbf{j}_i - \frac{en_e}{\nu_e} \sum_{s=1}^L \nu_{es} \mathbf{u}_s \quad (\text{Eq. 2})$$

where $\nu_e = \sum_{s=1}^L \nu_{es}$ is the total electron momentum transfer collision frequency. This driving current assumes the meaning of the classical ion slip term, when dealing only with a single population for both ions and neutrals (in such case, if ions and neutrals share the same fluid velocity, the driving current is zero, hence the term *ion slip*).

Introducing the electrostatic potential ϕ , and using the driving current of Eq. 2, the momentum balance equation can be rewritten as:

$$0 = -\nabla \cdot \mathcal{P}_e + en_e \nabla \phi + \mathbf{j}_e \times \mathbf{B} + \frac{m_e \nu_e}{e} (\mathbf{j} - \mathbf{j}_d) \quad (\text{Eq. 3})$$

where $\mathbf{j} = \mathbf{j}_e + \mathbf{j}_i$ is the total electric current density.

Let $\mathbf{1}_b = [b_1, b_2, b_3]$ be the unit vector along the applied magnetic field, so that $\mathbf{B} = B \mathbf{1}_b$, and $\omega_{ce} = eB/m_e$ the electron gyrofrequency. Then, Eq. 3 becomes:

$$0 = -\nabla \cdot \mathcal{P}_e + en_e \nabla \phi + \frac{m_e \omega_{ce}}{e} (\mathbf{j} - \mathbf{j}_i) \times \mathbf{1}_b + \frac{m_e \nu_e}{e} (\mathbf{j} - \mathbf{j}_d) \quad (\text{Eq. 4})$$

Introducing the Hall parameter $\chi = \omega_{ce}/\nu_e$, and the electron scalar conductivity $\sigma_e = e^2 n_e / (m_e \nu_e)$, Eq. 4

takes the form:

$$\mathbf{j} + \chi (\mathbf{j} \times \mathbf{1}_b) = \sigma_e \left(\frac{\nabla \cdot \mathcal{P}_e}{en_e} - \nabla \phi \right) + (\mathbf{j}_d + \chi \mathbf{j}_i \times \mathbf{1}_b) \quad (\text{Eq. 5})$$

Introducing the normalized conductivity tensor $\tilde{\mathcal{K}}$, for which $\tilde{\mathcal{K}}^{-1} \mathbf{j} = \mathbf{j} + \chi (\mathbf{j} \times \mathbf{1}_b)$,

$$\tilde{\mathcal{K}}^{-1} = \begin{bmatrix} 1 & \chi b_3 & -\chi b_2 \\ -\chi b_3 & 1 & \chi b_1 \\ \chi b_2 & -\chi b_1 & 1 \end{bmatrix}, \quad (\text{Eq. 6})$$

we can then write the total electric current density as:

$$\mathbf{j} = \mathcal{K} \cdot \left(\frac{\nabla \cdot \mathcal{P}_e}{en_e} - \nabla \phi \right) + \mathbf{j}_{\text{PIC}} \quad (\text{Eq. 7})$$

where $\mathcal{K} = \sigma_e \tilde{\mathcal{K}}$ is the conductivity tensor, and

$$\mathbf{j}_{\text{PIC}} = \tilde{\mathcal{K}} \cdot (\mathbf{j}_d + \chi \mathbf{j}_i \times \mathbf{1}_b) \quad (\text{Eq. 8})$$

is a known quantity obtained from the PIC sub-model. In fact, assuming quasineutrality $n_e = \sum_s Z_s n_s$ and a fluid closure for the electron temperature of the type $T_e = T_e(n_e)$, then both ν_e and σ_e are a function of the heavy species properties. In non-neutral simulations, on the other hand, the electron properties n_e and T_e are obtained by solving a coupled non-linear Poisson equation [29].

Assuming isotropic electrons, $\nabla \cdot \mathcal{P}_e = \nabla p_e$, with p_e the scalar electron pressure, we can then introduce a barotropy function h_e , such that $\nabla h_e = \nabla p_e / n_e$. For the special case of a polytropic electrons closure, as considered here, h_e takes the form:

$$h_e(n_e) = \begin{cases} T_{e0} \ln \left(\frac{n_e}{n_{e0}} \right), & \gamma = 1 \\ -\frac{\gamma T_{e0}}{(\gamma - 1)} \left[1 - \left(\frac{n_e}{n_{e0}} \right)^{\gamma - 1} \right], & \gamma > 1 \end{cases}, \quad (\text{Eq. 9})$$

where γ is the electron polytropic coefficient, and n_{e0} , T_{e0} are the electron density and temperature where h_e is set to zero.

Introducing the electron Bernoulli function H_e , satisfying $\nabla H_e = \nabla h_e - e \nabla \phi$, Eq. 7 finally reads

$$\mathbf{j} = \mathcal{K} \cdot \nabla H_e / e + \mathbf{j}_{\text{PIC}} \quad (\text{Eq. 10})$$

In the steady state, the total current density \mathbf{j} satisfies the continuity equation

$$\nabla \cdot \mathbf{j} = 0, \quad (\text{Eq. 11})$$

which is an elliptic equation for H_e :

$$\mathcal{K} : \nabla \nabla H_e + \nabla H_e \cdot (\nabla \cdot \mathcal{K}) = -e \nabla \cdot \mathbf{j}_{\text{PIC}} \quad (\text{Eq. 12})$$

where $\nabla \nabla H_e$ is the tensor Hessian of the Bernoulli function, and $\nabla \cdot \mathcal{K}$ is the divergence of the tensor

conductivity (a one-dimensional vector).

As the magnetic field magnitude tends to zero, the normalized conductivity tensor tends to the identity tensor $\tilde{\mathcal{K}} \rightarrow \mathcal{I}$, the right hand side current density tends to the driving current density $\mathbf{j}_{\text{PIC}} \rightarrow \mathbf{j}_d$, and Eq. 12 tends to the unmagnetized elliptic equation discussed in Ref. 29:

$$\nabla^2 H_e + \nabla H_e \cdot \nabla \ln(\sigma_e) = -\frac{e\nabla \cdot \mathbf{j}_d}{\sigma_e} \quad (\text{Eq. 13})$$

Once H_e has been solved for, it is possible to obtain the electric current density using Eq. 10, and finally the electric potential ϕ as:

$$\phi = \frac{h_e - H_e}{e}, \quad (\text{Eq. 14})$$

where we have chosen the same reference point for the electric potential, the barotropy function and the Bernoulli function ($H_e = h_e = 0$ where $\phi = 0$). The Bernoulli function H_e can thus be interpreted as the electric potential correction to be applied to the Boltzmann relation (or its extension to polytropic non-isothermal electrons), which neglects both magnetic and collisional effects on the electron momentum balance equation. It is finally underlined that the near-totality of the existing plume codes implicitly assume $H_e \equiv 0$.

2.1. Boundary conditions

In order to solve Eq. 12, we set without loss of generality $H_e = 0$ at one point (e.g. the reference point for the electron properties of the polytropic closure), and prescribe the value of a directional derivative at the boundaries of the simulation domain.

In stationary conditions, the Gauss theorem applied to the simulation volume with $\nabla \cdot \mathbf{j} = 0$, urges that the total net current through the simulation boundary be zero. It is noticed that this condition is valid even during transient conditions, if quasineutrality is assumed ($\rho_c = 0$).

A *strong* closure, which satisfies this integral relation, is to impose that the current density be exactly zero at all boundary nodes. If $\mathbf{1}_\perp$ is the normal unit vector at the boundaries, directed towards the plasma domain, this is equivalent to imposing:

$$\left(\tilde{\mathcal{K}} \cdot \nabla H_e\right) \cdot \mathbf{1}_\perp = -e \frac{\mathbf{j}_{\text{PIC}} \cdot \mathbf{1}_\perp}{\sigma_e} \quad (\text{Eq. 15})$$

Eq. 15 imposes the directional derivative of H_e along the direction $\tilde{\mathcal{K}}^T \mathbf{1}_\perp$, which is generally different from the boundary normal direction (and tends to it when $B \rightarrow 0$).

3. NUMERICAL SIMULATIONS

3.1. Simulation cases and settings

The simulations feature a quasineutral plasma plume injected symmetrically around the z axis, at an initial plane $z = 0$, and expanding downstream. Four plume cases are considered and differ only in terms of the magnetic field:

- Case 0: null magnetic field.
- Case 1: axial magnetic field $\mathbf{1}_b = [0, 0, 1]$.
- Case 2: magnetic field at 30 deg with the plume axis $\mathbf{1}_b = [1/2, 0, \sqrt{3}/2]$.
- Case 3: magnetic field at 60 deg with the plume axis $\mathbf{1}_b = [\sqrt{3}/2, 0, 1/2]$.

The magnetic field magnitude for Cases 1 to 3 is set to 0.1 Gauss, while the rest of simulation parameters is reported in Table 1.

Both Xe ions and neutrals are injected from the $z = 0$ plane, from a circular area with center at $x = y = 0$ and radius 0.3 m. Regarding the former, they are injected with an initial profile given by the Self-Similar Parks-Katz plume profile [6, 7] (Gaussian radial density profile), with an axial velocity of 25 km/s, a zero divergence angle, a 95% ion current radius of 0.15 m and a peak flux at $x = y = 0$ of $6.0 \cdot 10^{20} \text{ m}^{-2} \text{ s}^{-1}$. The neutrals, on the other hand, feature a uniform injection (constant density over the injection surface) with a flux of $2.5 \cdot 10^{20} \text{ m}^{-2} \text{ s}^{-1}$, an axial velocity of 350 m/s, and a zero divergence. The injection temperature for both ions and neutrals is 0.1 eV (this makes the neutrals sonic at injection). The considered collisions are charge-exchange (CEX) collisions (between injected ions and neutrals) and the first ionization reaction of Xe neutrals ($\text{Xe} + e \rightarrow \text{Xe}^+ + 2e$), which are both modeled as described in Ref. 29.

For what concerns the electron fluid model, the polytropic closure is based on a reference electron temperature $T_{e0} = 3 \text{ eV}$ at $x = y = z = 0$ (which is the reference point also for electric potential and Bernoulli function), and on a polytropic cooling coefficient $\gamma = 1.2$, which yields a mild cooling downstream. Furthermore, for the computation of the electron collision frequency ν_e , appearing in the definition of the scalar conductivity σ_e , a minimum background neutrals density is considered, equal to $1 \cdot 10^{16} \text{ m}^{-3}$, while the Hall parameter χ is limited to a maximum value of 50, in order to guarantee a correct convergence of the fluid solver. In fact, as the Hall parameter grows, the condition number of the linear system increases, making the solver convergence more challenging.

The simulation duration is 1.76 ms (enough to fill the simulation domain with injected neutrals), while the time-step is 1.6 μs . Of the total 11000 time steps, only the final 1000 steps are run with the fluid solver, in order to speed up the simulation. In order to reduce the input noise to this solver, the input plume properties from the PIC sub-model are time-averaged over 500 time steps. This represents no limitation in the current scenario, since the steady state solution is expected to be non-oscillating. Finally, the simulation domain is a parallelepiped of 1.6 m side along x and y , and 4 m side with along z , featuring $81 \times 81 \times 101$ computational nodes (along x , y and z). This means that the PIC cell is 2 cm wide along x and y , and 4 cm wide along z .

Table 1: Simulation parameters.

Simulation parameters	Units	Values
Max. injection radius for ions/neutrals	m	0.3
Injected ions profile	n/a	Parks-Katz [7]
Injected peak ion flux	$\text{m}^{-2}\text{s}^{-1}$	$6 \cdot 10^{20}$
95% ion current radius	m	0.15
Ions injection axial velocity	km/s	25.0
Ions initial divergence angle	deg	0.0
Injected neutrals profile	n/a	Flat
Injected neutrals flux	$\text{m}^{-2}\text{s}^{-1}$	$2.5 \cdot 10^{20}$
Neutrals injection axial velocity	km/s	0.35
Neutrals initial divergence angle	deg	0.0
Ions/neutrals injection temperature	eV	0.1
Considered heavy particles collisions	n/a	CEX and ionization
Reference electron temperature	eV	3.0
Electron polytropic cooling coefficient	n/a	1.2
Background neutrals density	m^{-3}	$1 \cdot 10^{16}$
Upper threshold for the Hall parameter	n/a	50
PIC time-step	s	$1.6 \cdot 10^{-6}$
Simulation duration	s	$1.76 \cdot 10^{-3}$
Time-averaging steps for PIC sub-model	n/a	500
Simulation domain physical dimensions	m	$1.6 \times 1.6 \times 4.0$
Number of computational nodes per dimension	n/a	$81 \times 81 \times 101$

3.2. Simulation results

The unmagnetized case 0 represents the comparison baseline case, with which the magnetized plume cases 1 to 3 are compared. Therefore, simulation results are presented for this case first.

Case 0: unmagnetized case

The total ion density is shown, for a $y = 0$ cross section (which contains the plume axis), in Fig. 1 (a). It presents a peak value slightly above $2 \cdot 10^{16} \text{ m}^{-3}$, a bit downstream from the injection plane, because of the effect of CEX ions. Then the ion density starts to decrease as the ion divergence angle increases due to the effect of the ambipolar electric field. The cloud of slow CEX ions, surrounding the plume core, can also be appreciated, with a density higher than 10^{14} m^{-3} . CEX ions are then either accelerated radially outwards or towards the injection plane (ion backflow). Since the simulations assume quasi-neutrality and no doubly-charged ions are considered, the electron density coincides with the ion density.

Fig. 1 (b) shows the Xe neutral density. Neutrals expand almost spherically downstream and present peak densities above 10^{17} m^{-3} at the injection plane. Then their density quickly drops below 10^{16} m^{-3} , at distances larger than 2 m from the injection plane.

Fig. 1 (c) shows the electron temperature distribution, still at the $y = 0$ plane. The reference value of 3.0 eV can be appreciated at the injection plane centerline, and, as the density decreases, a mild cooling is simulated with temperatures dropping to values as low as 0.5 eV downstream and radially outwards.

The combined effect of electron temperature and heavy species densities can be appreciated in Fig. 1 (d) showing the electron scalar conductivity σ_e . This features a peak value around $2500 \Omega^{-1}\text{m}^{-1}$, decreases downstream and presents values around $500 \Omega^{-1}\text{m}^{-1}$, in the lateral regions of the plasma plume, populated by CEX ions.

In this unmagnetized plume case, the Bernoulli function H_e can be obtained by solving Eq. 13. The driving current density j_d , equal to j_{PIC} since $B = 0$, and the solution for H_e are shown respectively in Fig. 2 (a) and (b). Since the plasma plume is lowly collisional, as expected, the electric potential correction due to collisions (given by $-H_e/e$, Eq. 14), is quite small, limited to a few mV. The consequent electric potential and electric field are shown in Fig. 2 (c) and (d), and nearly coincide with the collisionless polytropic solution. The electric potential assumes the reference value of 0 at the reference

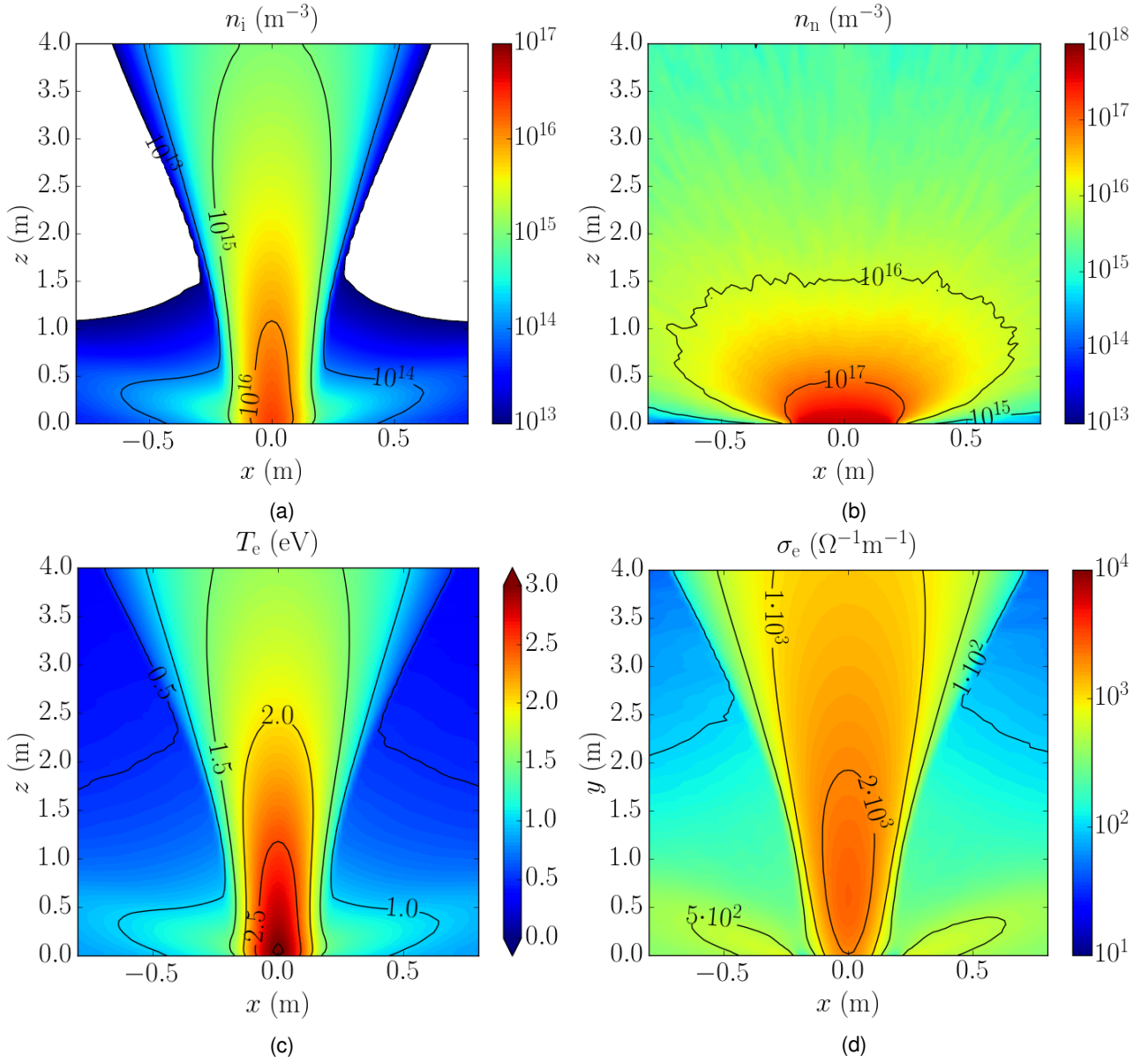


Figure 1: Unmagnetized plume simulation results at $y = 0$: (a) ion density, (b) neutrals density, (c) polytopic electron temperature, and (d) electron scalar conductivity.

point for electron properties (electron density and temperature) and decreases by approximately 6 V in 4 m along the centerline. For what concerns the electric field, this shows the typical shape of an expanding plasma plume, with a small axial field at the centerline (which further accelerates the ions) and a much stronger radial electric field which pushes the CEX ions outwards. Close to the injection plane $z = 0$, the electric field is directed backwards, thus producing the expected CEX ions backflow.

The electric current density is finally shown in Fig. 2 (e) and (f) in respectively the $y = 0$ and $z = 2$ m planes. Such electric current is predominantly axial, presents a peak value around 10 A/m² and drops rapidly downstream. The plasma plume is not perfectly current-free because a non-zero driving cur-

rent j_d is present (Eq. 2), generated by the ion slip with respect to the neutral population ($u_i \gg u_n$).

Case 1: Axial magnetic field

In this case, a magnetic field of 0.1 Gauss magnitude is applied parallel to the plasma plume axis. As a result, no asymmetry in the plume solution is expected, although the reduced radial electron mobility should induce a focusing effect on the plume ions. Results are shown in Fig. 3 (a) to (f).

The PIC current density vector j_{PIC} is shown in both magnitude and direction in Fig. 3 (a). Values up to 40 A/m² are found at the injection plane and quickly reduce to fractions of A/m² downstream. Observe that j_{PIC} is perfectly symmetric with respect to the

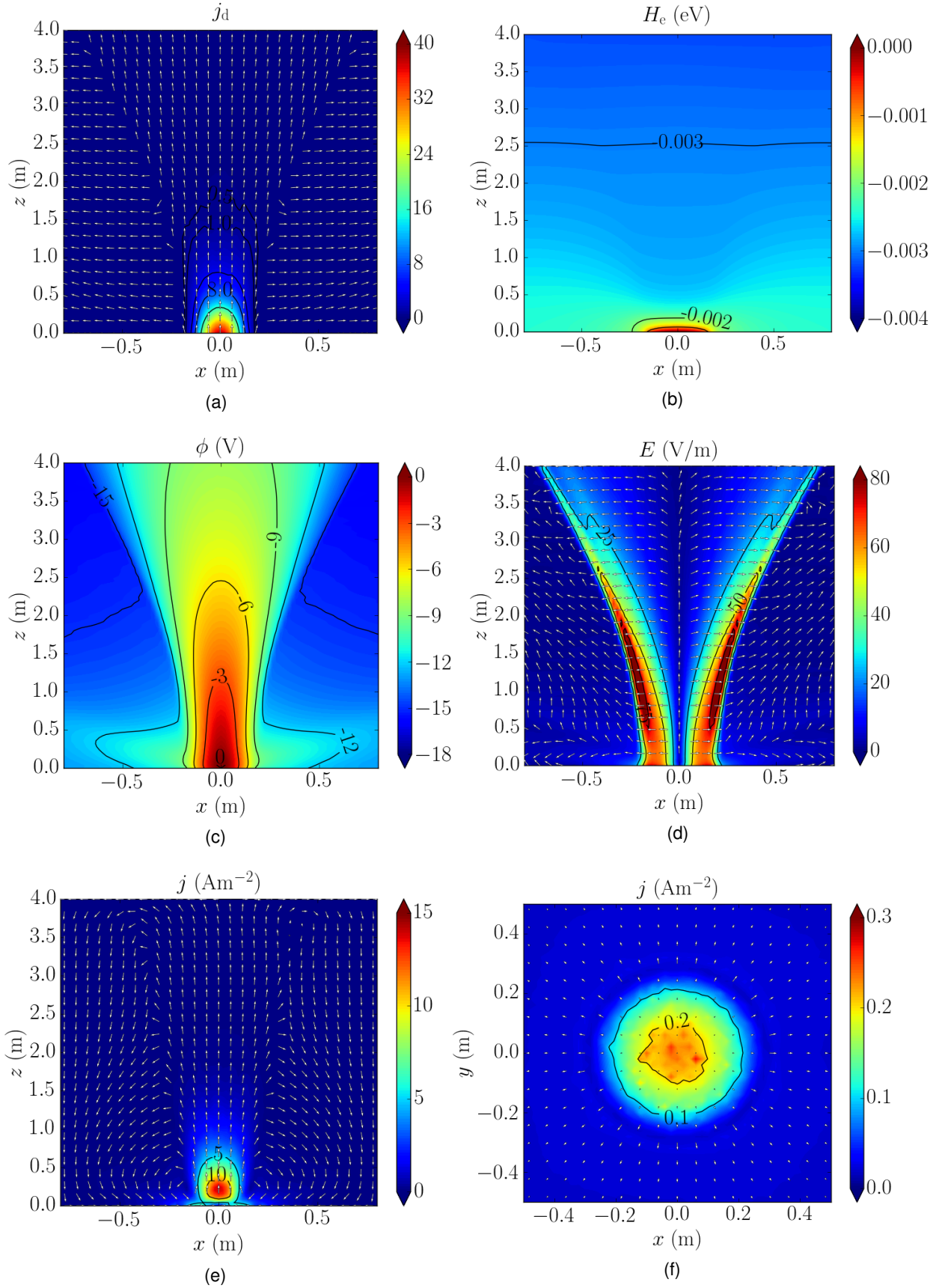


Figure 2: Unmagnetized plume simulation results: (a) driving current density at $y = 0$, (b) Bernoulli function at $y = 0$, (c) electric potential at $y = 0$, (d) electric field at $y = 0$, (e) electric current density at $y = 0$, and (f) electric current density at $z = 2\text{m}$. In subplots (a), (d), (e) and (f), the arrows show the direction of the vector in the considered plane, while their length is proportional to the ratio between the in-plane magnitude and the total magnitude.

plume axis and directed along it (except in the lateral plume regions, where it is driven by CEX ions).

The Hall parameter is shown in Fig. 3 (b), and it shows a minimum value at the injection plane centerline around 5. As the plasma density and neutral density decrease downstream, the Hall parameter tends to increase, up to the maximum allowed value (50). It is underlined that the Hall parameter grows monotonically as we go farther downstream and the plume approaches a collisionless state.

The solution of Eq. 12 is then shown at both $y = 0$ and $z = 0$, in Fig. 3 (c) and (d). Its dependency on z is small and a clear axisymmetric shape is found, as easily predictable for this axisymmetric case (axial magnetic field). Moreover H_e is negative everywhere, meaning that the correction to the polytropic potential solution is positive (refer to Eq. 14), and increasing radially outwards. This means a lower electric potential fall or a lower radial electric field with respect to the unmagnetized case. The latter can even invert direction and become inwards, starting from a minimum downstream distance that depends on the plume properties and on the magnetic field magnitude. In fact, the radial gradient of the polytropic electron potential solution decreases monotonically with z and, at some point, it becomes lower than the radial gradient of the H_e function. This focusing effect of the magnetic field can be explained by considering the decreased electron mobility in the cross-field direction (in this case in the radial direction). When the Hall parameter becomes very large and the plume nearly collisionless, electrons are bound to the axial magnetic field lines and cannot traverse radially the plume, so that ions must stop diverging too. This requires the onset of a focusing electric field. At small distances from the plume injection plane, on the other hand, the polytropic electric potential gradient clearly dominates, and the electric field is still directed outwards, as in unmagnetized plasma plumes.

The electric current density, given by Eq. 10, is then shown in Fig. 3 (e) and (f) and reaches a maximum value around 25 A/m² downstream. This current is mostly azimuthal, except at the plume centerline where it is axial, and it is also diamagnetic, as the induced magnetic field (along $-z$ and not treated here) is opposite to the external imposed one (along $+z$).

Cases 2 and 3: Magnetic field at 30 and 60 deg

In cases 2 and 3, a magnetic field of magnitude 0.1 Gauss, is applied in the $x - z$ plane with an angle of respectively 30 and 60 deg with respect to the plume axis. This geometric configuration is expected to introduce important asymmetries in the

plasma plume properties. Results in terms of the Bernoulli function and of the induced electron currents are shown in Figs. 4 and 5.

When the magnetic field is at an angle with the plume axis, the cross product $\mathbf{j}_i \times \mathbf{1}_b$ appearing in the PIC current density expression is what introduces an asymmetry in the right hand side of Eq. 12. As a consequence, the H_e solution is strongly asymmetric and affected by the direction of the external magnetic field, as shown in Fig. 4 (a) to (d) for both cases 2 and 3.

Fig. 4 (a) shows the Bernoulli function at $y = 0$ for case 2. The corresponding magnetic field, belonging to this $x - z$ plane and forming an angle of 30 deg with the plume axis, tends to hinder the expansion along the in-plane direction normal to $\mathbf{1}_b$, so that H_e is nearly constant along $\mathbf{1}_b$ and negative almost everywhere. At a larger magnetic field angle (with respect to the plume axis) of 60 deg (Fig. 4 (b)), the same considerations hold, with more oblique isopotential lines for H_e . As already shown in Fig. 3 (e) and (f), this generates a circulating diamagnetic current around the magnetic field direction, which in this case is no more azimuthal but presents a non-negligible axial component.

Fig. 4 (c) and (d) then show the H_e solution at $x = 0$ for respectively cases 2 and 3. Here, the expanding plume shape can be better appreciated, together with a small boundary conditions effect. In fact, close to the final z cross section, the y gradient of the H_e function decreases at the plume centerline, in order to comply with the $\mathbf{j} \cdot \mathbf{1}_\perp = 0$ condition. This means that the magnetic field effects might be badly modeled in these final expansion region. An important observation is that the electric potential correction due to the magnetic field (which goes as $-H_e$) compensates nearly completely the deviating effect of the Lorentz force. In fact, ions suffer a Lorentz force along the $+y$ direction given by $+e\mathbf{v}_z B_x$. The compensation electric force (due to the Bernoulli function) can be computed as $+(1/e)\partial H_e/\partial y$, and the two contributions nearly balance each other at low plume radii. At larger radii, the H_e correction becomes negative everywhere (with an inwards gradient), thus yielding again a focusing effect. As a consequence of these simultaneous effects of the electric field, the plasma plume cross section deforms, and in particular it is compressed in the cross-field direction (i.e. along y). At the same time, the deviation of the plasma plume is small, if not negligible, as already suggested by previous theoretical work [6].

The electric current density at $x = 0$ and at $z = 2$ m is shown for both simulation cases in Fig. 5 (a) to (d). Fig. 5 (a) shows such current at $x = 0$ for

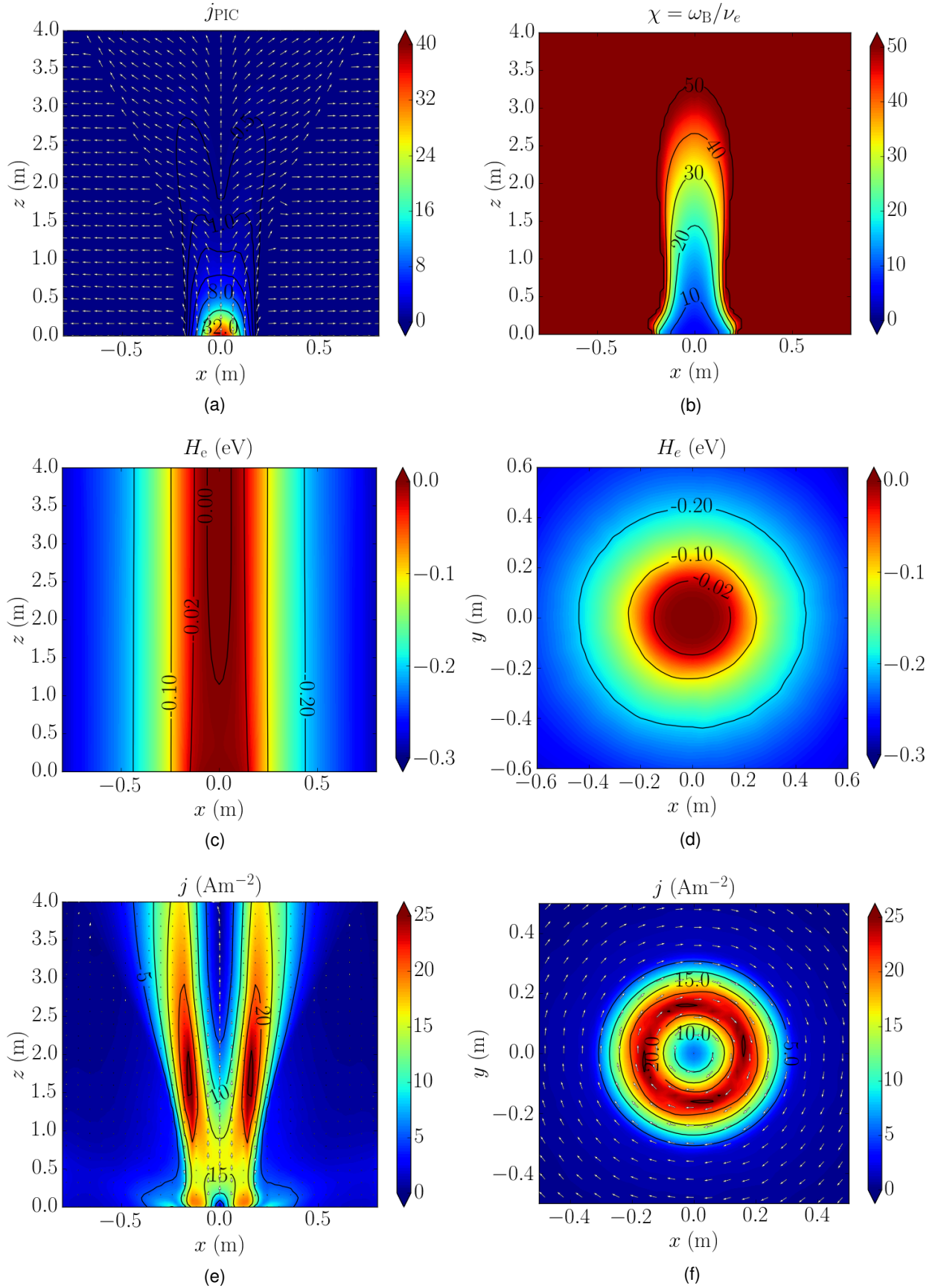


Figure 3: Axial magnetic field simulation results: (a) PIC current density, at $y = 0$, (b) Hall parameter at $y = 0$, (c) Bernoulli function at $y = 0$, (d) Bernoulli function at $z = 0$, (e) electric current density at $y = 0$, and (f) electric current density at $z = 2$ m. In subplots (a), (e) and (f), the arrows show the direction of the vector in the considered plane, while their length is proportional to the ratio between the in-plane magnitude and the total magnitude.

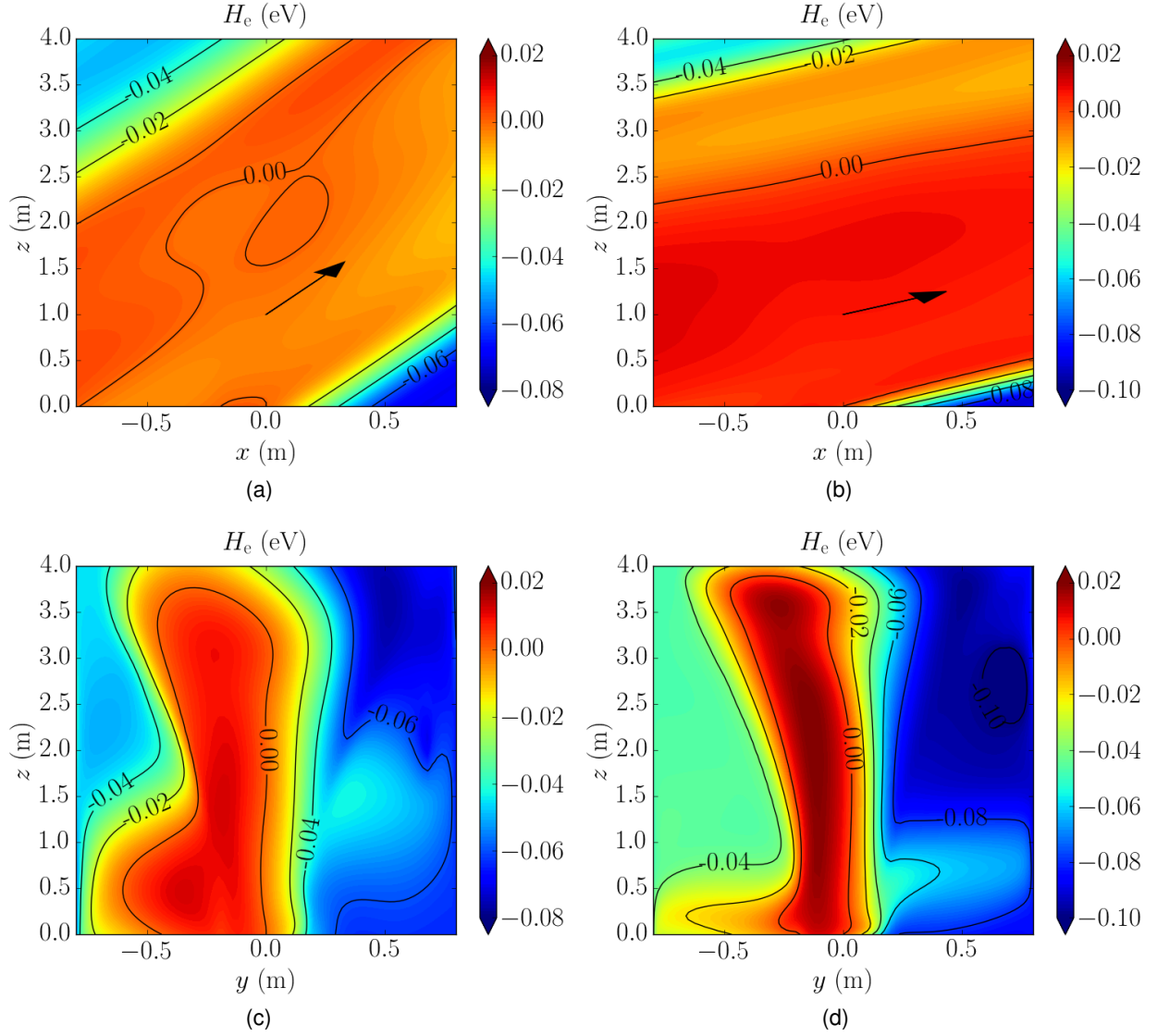


Figure 4: Oblique magnetic field cases: Bernoulli function at $y = 0$ for (a) case 2 and (b) case 3. Bernoulli function at $x = 0$ for (c) case 2, and (d) case 3. In subplots (a) and (b), the magnetic field direction $\mathbf{1}_b$ is shown by a black arrow. Case 2 features $\mathbf{1}_b = [1/2, 0, \sqrt{3}/2]$ (30 deg inclination), while case 3 features $\mathbf{1}_b = [\sqrt{3}/2, 0, 1/2]$ (60 deg inclination).

case 2 (the magnetic field has a positive component towards the reader). A complex diamagnetic and three-dimensional electric current loop forms. The plume centerline is almost current-free, while two opposite layers of opposite current can be appreciated, as clearly visible in Fig. 5 (c), which shows the axial component of the electric current density at a mid-distance cross section ($z = 2$ m). Since the plume is locally divergent-free, the amount of current circulating in the positive z direction must match the amount of current circulating along $-z$. This current loop is once again diamagnetic as it produces an induced magnetic field with a component along $-x$. A similar electric current density is found for the higher magnetic field angle case (case 3), shown in Fig. 5 (b) and (d). In this case, the electric current density presents a slightly more symmetric shape around the $+x$ direction, and it is also larger than in

case 2 (approximately by a factor of 2), with peak values of more than 20 A/m² close to the injection plane (this is an in-plane current, as $j_z = 0$ at $z = 0$, due to the imposed boundary conditions).

3.3. Effects of the external magnetic field on the plasma plume density

The H_e solution is coupled, through the electric potential ϕ (Eq. 14), with the ion macro-particles motion and dynamics, simulated by the PIC submodule. Fig. 6 (a) to (f) show the effects of the magnetic field on the plasma plume expansion, in terms of the ion density relative variation with respect to the unmagnetized plume case 0. This is done for the magnetized plume cases 1 to 3, at two different planes: the symmetry plane $x = 0$ and the

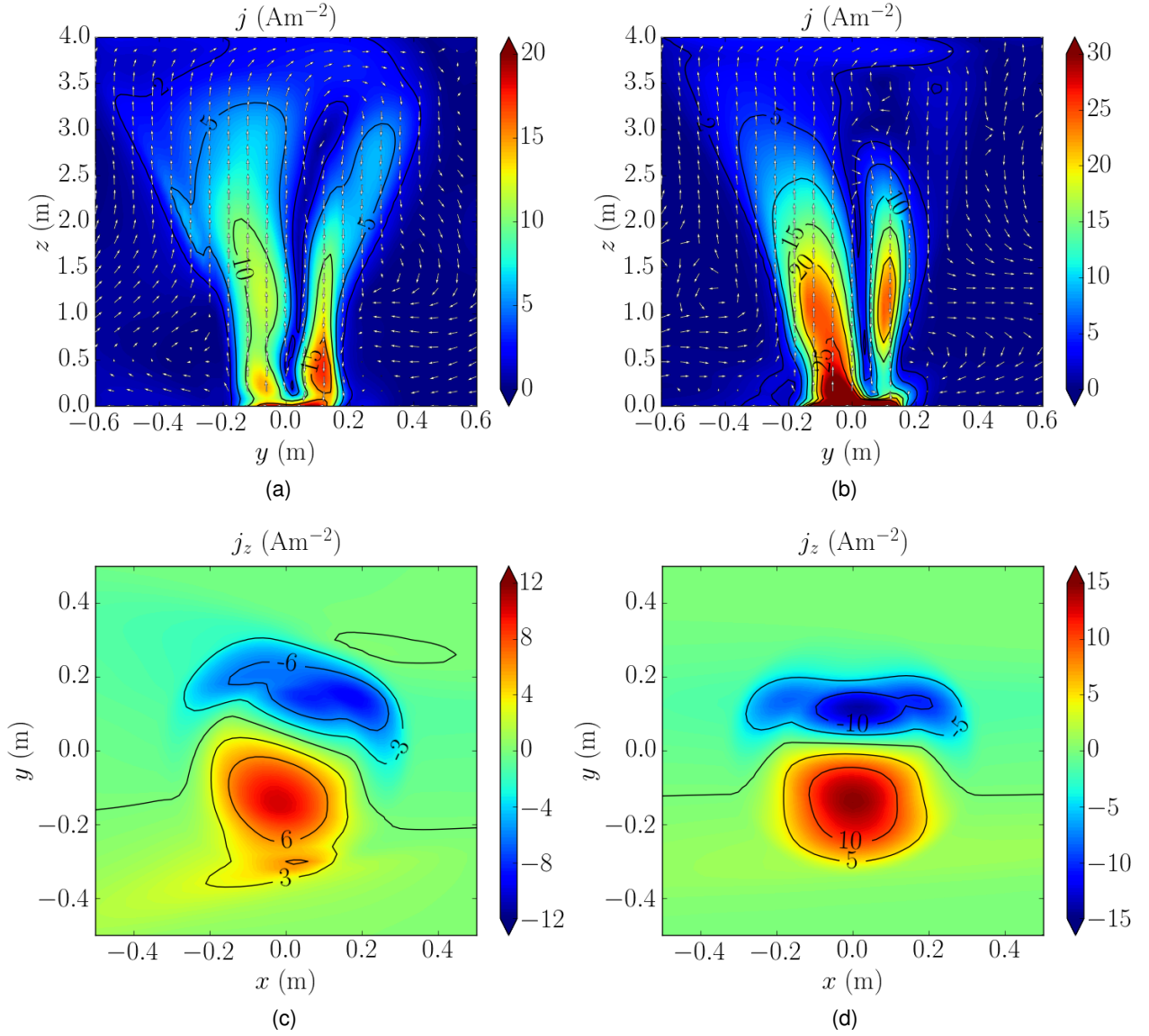


Figure 5: Oblique magnetic field cases: electric current density at $x = 0$ for (a) case 2 and (b) case 3. z component of the electric current density, at $z = 2$ m, for (c) case 2, and (d) case 3. Case 2 features a magnetic field direction $\mathbf{1}_b = [1/2, 0, \sqrt{3}/2]$ (30 deg inclination), while case 3 features $\mathbf{1}_b = [\sqrt{3}/2, 0, 1/2]$ (60 deg inclination).

final cross section $z = 4$ m.

In the axial magnetic field case (subplots (a) and (b)), the effect of the magnetic field is to focus the plasma plume expansion, so that the plume ions tend to diverge less than in the unmagnetized plume case. This yields to a slight increase of the density of about 1%, at low radii of the final cross section, and to a larger relative drop in density at the periphery of the unmagnetized plume case (the more focused magnetized plume ions in fact diverge less and do not reach such regions). The CEX ions, on the other hand, show a mild increase in density (up to 2-3%) around the main plume core, because of the lower radial electric fields, which naturally tend to push them outwards.

In cases 2 and 3, shown respectively in subplots (c), (d), and (e), (f), the oblique magnetic field produces a non-axisymmetric plasma plume, as it expands downstream. The non-axisymmetric force contributions, which are responsible of this phenomenon, are (i) the deflecting Lorentz force, which now has a positive component along y , and (ii) the electric field component due to the limited electron mobility (i.e. the Bernoulli energy function gradient). At the considered ion injection velocities (25 km/s), magnetic fields (0.1 Gauss), and angles between plume axis and magnetic field (30 and 60 deg), the ion gyromotion radius is in the order of a few km, yielding a $+y$ deflection in the order of mm at the final cross section. As commented above, however, the effect of the Bernoulli function gradient is to compensate such deflection with an opposite and nearly equal

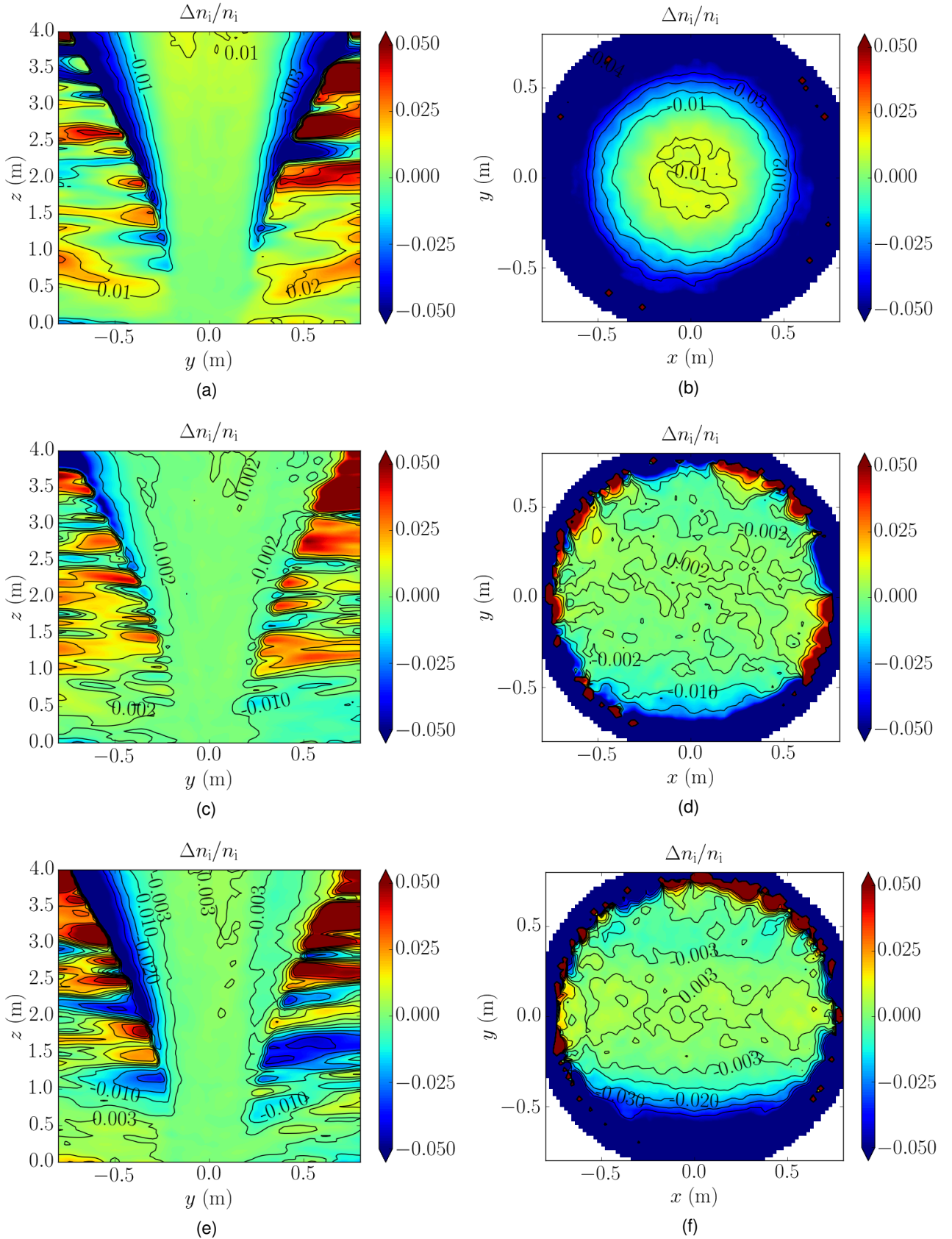


Figure 6: Relative change in ion density, due to the magnetic field, at $x = 0$ (subplots (a), (c) and (e)) and $z = 4$ m (subplots (b), (d) and (f)), for case 1 (subplots (a) and (b)), case 2 (subplots (c) and (d)), and case 3 (subplots (e) and (f)). Subplots (b), (d) and (f) only show the density change for the injected ions, while subplots (a), (c) and (e) show the total ion density change (including CEX ions). Case 1 features an axial magnetic field $\mathbf{1}_b = [0, 0, 1]$, case 2 features $\mathbf{1}_b = [1/2, 0, \sqrt{3}/2]$ (30 deg inclination), while case 3 features $\mathbf{1}_b = [\sqrt{3}/2, 0, 1/2]$ (60 deg inclination).

force, so that no net displacement of the plasma plume center of mass is expected [6].

Fig. 6 (c) and (d) show the ion density change due to the magnetic field in case 2 (30 deg angle). Referring to the final cross section (subplot (d)), it is apparent that the plume cross section is compressed along the y direction, so that the density change is positive, on average, along the $y = 0$ direction (i.e. along the projection of the magnetic field vector on the considered plane) and negative at larger $|y|$ values. For what concerns the ion density change in the $x = 0$ plane (subplot (c)), the compression along y is again visible, while the effects on the CEX ions density are less evident than in the axial field case. Regarding the plume deflection along y this is almost negligible too, so that our theoretical predictions of a zero net plume deflection are confirmed.

A similar behavior is found for case 3, shown in Fig. 6 (e) and (f). The main difference is that now the changes are larger (by at least a factor of 2 with respect to case 2) and the plume compression along y is more evident. The net plume deflection along y finally remains negligible.

3.4. Induced magnetic field

The diamagnetic plasma currents of the magnetized plume cases generate an induced magnetic field that opposes the external one. The strength of this induced field can be roughly estimated from Ampere's law as $B_{\text{ind}} \approx L\mu_0 j$, where μ_0 is the magnetic permeability of a vacuum and L is a characteristic size of the plasma plume. Assuming a current density of 10 A/m^2 , and a characteristic plume diameter of 0.5 m , then the induced magnetic field turns out to be 0.06 Gauss . This magnitude is comparable to that of the external magnetic field (0.1 Gauss), so that the effects of the induced field are not negligible. Nevertheless, the exact computation of the induced field and the study of its effects on the plume expansion are left to future studies.

4. CONCLUSIONS AND FUTURE WORK

This paper has presented an electron fluid model dedicated to study magnetized plasma plume expansions. A previously presented model, which already considered the effect of electron collisions with the heavy particles (ions and neutrals), has been extended to include the effects of the magnetic field, with the introduction of a tensor conductivity. The new model computes a correction to the collisionless and unmagnetized plume solution, in the form of a Bernoulli function, which takes into account the effects of both collisions and magnetization.

In order to investigate the effects of a magnetic field on a plasma plume expansion, a set of four simulations has been carried out, including a reference unmagnetized case for comparison. The effects of the external magnetic field have been identified in terms of the induced electric currents in the plume and of the induced changes in the ion density profiles. It has been found that an axial magnetic field focuses the plume ions, by reducing their divergence increase along the expansion, and also generates azimuthal diamagnetic electric currents.

When the magnetic field is at an angle with the plume axis, on the other hand, complex electric current structures appear, which remain, nevertheless, diamagnetic in character with respect to the applied magnetic field. Moreover, the electric potential correction has the additional effect of counteracting the Lorentz force deviation of the core plume ions and to induce a deformation of the plume cross section downstream. As a consequence, the cross section seems to compress in the cross-field direction, as shown by Korsun [32], and the net deflection of the ion plume is almost negligible, as also demonstrated theoretically with an integral argument for a plasma plume inside a uniform magnetic field [6]. In fact, if no net current exits the boundaries, the integral Lorentz force on the ions should perfectly balance the total force on the electrons.

In all magnetized plume cases, an approximate order of magnitude analysis has finally shown that the induced magnetic field, generated by the diamagnetic plasma currents, is of the same order of magnitude of the external one, so that its effects might not be negligible.

Future work shall focus on the following topics: (i) the demonstration that the integral force transferred by the external magnetic field to the plasma plume is indeed zero, (ii) the detailed analysis of the three-dimensional electric current structures, (iii) plume simulations with non-uniform and larger magnetic fields, like that of a magnetic nozzle, and (iv) the study of self-consistent plasma plume expansions, taking into account the effects of the induced magnetic field.

ACKNOWLEDGMENTS

The research has been funded by the Spain's R&D National Plan, grant agreement ESP2016-75887.

REFERENCES

- [1] Bombardelli, C. and Peláez, J., "Ion Beam Shepherd for Contactless Space Debris Removal," *Journal of Guidance, Control, and Dynamics*, Vol. 34, No. 3, 2011, pp. 916–920.

- [2] Bombardelli, C., Urrutxua, H., Merino, M., Ahedo, E., and Peláez, J., "Relative Dynamics and Control of an Ion Beam Shepherd Satellite," *Advances in the Astronautical Sciences, proceedings of Space Flight Mechanics conference 2012*, Vol. 143, Univelt, Inc., 2012, pp. 2145–2158.
- [3] Bombardelli, C., Urrutxua, H., Merino, M., Ahedo, E., and Peláez, J., "The ion beam shepherd: A new concept for asteroid deflection," *Acta Astronautica*, Vol. 90, No. 1, 2013, pp. 98–102.
- [4] Merino, M., Ahedo, E., Bombardelli, C., Urrutxua, H., and Peláez, J., "Ion Beam Shepherd satellite for Space Debris Removal," *Progress in Propulsion Physics*, Vol. 4 of *EUCASS Advances in Aerospace Sciences*, EDP Sciences, Les Ulis, France, 2013, pp. 789–802.
- [5] Cichocki, F., Merino, M., and Ahedo, E., "Modeling and Simulation of EP Plasma Plume Expansion into Vacuum," *50th Joint Propulsion Conference*, paper 2014-3828, AIAA, Reston, VA, Cleveland, Ohio, July 28-30, 2014.
- [6] Merino, M., Cichocki, F., and Ahedo, E., "Collisionless Plasma thruster plume expansion model," *Plasma Sources Science and Technology*, Vol. 24, No. 3, 2015, pp. 035006.
- [7] Parks, D. and Katz, I., "A preliminary model of ion beam neutralization," *14th International Electric Propulsion Conference*, paper 1979-2049, Electric Rocket Propulsion Society, Fairview Park, OH, Princeton, New Jersey, October 30 - November 1, 1979.
- [8] Ashkenazy, J. and Fruchtman, A., "Plasma plume far field analysis," *27th International Electric Propulsion Conference*, paper 2001-260, Electric Rocket Propulsion Society, Fairview Park, OH, Pasadena, California, October 15-19, 2001.
- [9] Korsun, A. and Tverdokhlebova, E., "The characteristics of the EP exhaust plume in space," *33rd Joint Propulsion Conference and Exhibit*, paper 1997-3065, AIAA, Reston, VA, Seattle, Washington, July 6-9, 1997.
- [10] Ortega, A., Katz, I., Mikellides, I., and Goebel, D., "Self-Consistent Model of a High-Power Hall Thruster Plume," *IEEE Transactions on Plasma Science*, Vol. 43, No. 9, 2015, pp. 2875–2886.
- [11] Kahnfeld, D., *Hybrid Plume Modeling*, Master's thesis, Mathematisch-Naturwissenschaftliche Fakultät Ernst-Moritz-Arndt-Universität Greifswald, Greifswald, Germany, 2015.
- [12] Korkut, B. and Levin, D., "Three Dimensional DSMC-PIC Simulations of Ion Thruster Plumes with SUGAR," *50th Joint Propulsion Conference*, paper 2014-3447, AIAA, Reston, VA, Cleveland, Ohio, July 28–30, 2014.
- [13] Korkut, B., Li, Z., and Levin, D., "3-D Simulation of Ion Thruster Plumes Using Octree Adaptive Mesh Refinement," *IEEE Transactions on Plasma Science*, Vol. 43, No. 5, 2015, pp. 1706–1721.
- [14] Araki, S., Martin, R., Bilyeu, D., and Koo, J., "SM/MURF: Current Capabilities and Verification as a Replacement of AFRL Plume Simulation Tool COLISEUM," *52nd Joint Propulsion Conference*, paper 2016-4939, AIAA, Reston, VA, Salt Lake City, Utah, July 25-27, 2016.
- [15] Cai, C., "Numerical studies on plasma plume flows from a cluster of electric propulsion devices," *Aerospace Science and Technology*, Vol. 41, 2015, pp. 134–143.
- [16] Taccogna, F., Pagano, D., Scortecchi, F., and Garulli, A., "Three-dimensional plume simulation of multi-channel thruster configuration," *Plasma Sources Science and Technology*, Vol. 23, No. 6, 2014, pp. 065034.
- [17] Boyd, I. and Yim, J., "Hall thruster plume simulation using a detailed hybrid model," *40th Joint Propulsion Conference and Exhibit*, paper 2004-3952, AIAA, Reston, VA, 2004.
- [18] Celik, M., Santi, M., Cheng, S., Martínez-Sánchez, M., and Péraire, J., "Hybrid-PIC simulation of a Hall thruster plume on an unstructured grid with DSMC collisions," *28th International Electric Propulsion Conference*, paper 2003-134, Electric Rocket Propulsion Society, Fairview Park, OH, Toulouse, France, March 17-21, 2003.
- [19] Santi, M., *Hall thruster plume simulation using a hybrid-PIC algorithm*, Ph.D. thesis, Massachusetts Institute of Technology, Boston, MA, 2003.
- [20] Forest, J., Eliasson, L., and Hilgers, A., "A new spacecraft plasma simulation software, PicUp3D/SPIS," *7th Spacecraft Charging Technology Conference*, Vol. 476, The Netherlands, April 23-27, 2001, p. 515.
- [21] Masselin, M., *Development of a hybrid PIC code for the simulation of plasma spacecraft interactions*, Master's thesis, University of Stockholm, Sweden, 2012.
- [22] Wartelski, M., Theroude, C., Ardura, C., and Gengembre, E., "Self-consistent Simulations of Interactions Between Spacecraft and Plumes

of Electric Thrusters,” *33rd International Electric Propulsion Conference*, paper 2013-73, Electric Rocket Propulsion Society, Fairview Park, OH, Washington D.C., October 7-10, 2013.

- [23] Tskhakaya, D., Matyash, K., Schneider, R., and Taccogna, F., “The Particle-In-Cell Method,” *Contributions to Plasma Physics*, Vol. 47, No. 8-9, 2007, pp. 563–594.
- [24] Wang, H., Jiang, W., and Wang, Y., “Implicit and electrostatic particle-in-cell/Monte Carlo model in two-dimensional and axisymmetric geometry: I. Analysis of numerical techniques,” *Plasma Sources Science and Technology*, Vol. 19, No. 4, 2010, pp. 045023.
- [25] Wang, J., Chang, O., and Cao, Y., “Electron-Ion Coupling in Mesothermal Plasma Beam Emission: Full Particle PIC Simulations,” *IEEE Transactions on Plasma Science*, Vol. 40, No. 2, 2012, pp. 230–236.
- [26] Hu, Y. and Wang, J., “Fully kinetic simulations of collisionless, mesothermal plasma expansion,” *13th Spacecraft Charging Technology Conference*, Pasadena, California, June, 23-27, 2014.
- [27] Wang, J., Han, D., and Hu, Y., “Kinetic simulations of plasma plume potential in a vacuum chamber,” *IEEE Transactions on Plasma Science*, Vol. 43, No. 9, 2015, pp. 3047–3053.
- [28] Lapenta, G., “Automatic adaptive multi-dimensional particle-in-cell,” *Advanced Methods for Space Simulations*, 2007, pp. 61–76.
- [29] Cichocki, F., Domínguez, A., Merino, M., and Ahedo, E., “Hybrid 3D model for the interaction of plasma thruster plumes with nearby objects,” *Plasma Sources Science and Technology*, Vol. 26, No. 12, 2017, pp. 125008.
- [30] Cichocki, F., *Analysis of the expansion of a plasma thruster plume into vacuum*, Ph.D. thesis, Universidad Carlos III de Madrid (UC3M), Leganés, Spain, 2017.
- [31] Cichocki, F., Domínguez, A., Merino, M., and Ahedo, E., “A 3D hybrid code to study electric thruster plumes,” *Space Propulsion Conference*, paper 2016-3124968, 3AF, Paris, France, Rome, Italy, May 2-6, 2016.
- [32] Korsun, A., Tverdokhlebova, E., and Gabdullin, F., “Earth’s Magnetic Field Effect Upon Plasma Plume Expansion,” *25th International Electric Propulsion Conference*, paper 1997-178, Electric Rocket Propulsion Society, Fairview Park, OH, Cleveland, Ohio, August 24-28, 1997.